Viscoelasticity of basal plasma membranes and cortices derived from MDCK II cells

Andreas Janshoff[1,*]

[1]Department of Chemistry, Institute of Physical Chemistry, Göttingen

ABSTRACT The mechanical properties of cells are largely determined by the architecture and dynamics of their viscoelastic cortex, which consists of a contractile, cross-linked actin mesh attached to the plasma membrane via linker proteins. Measuring the mechanical properties of adherent, polarized epithelial cells is usually limited to the upper, i.e., apical side, of the cells because of their accessibility on culture dishes. Therefore, less is known about the viscoelastic properties of basal membranes. Here, I investigate the viscoelastic properties of basolateral membranes derived from polarized MDCK II epithelia in response to external deformation and compare them to living cells probed at the apical side. MDCK II cells were grown on porous surfaces to confluence, and the upper cell body was removed via a squirting-lysis protocol. The free-standing, defoliated basal membranes were subject to force indentation and relaxation experiments permitting a precise assessment of cortical viscoelasticity. A new theoretical framework to describe the force cycles is developed and applied to obtain the time-dependent area compressibility modulus of cell cortices from adherent cells. Compared with the viscoelastic response of living cells, the basolateral membranes are substantially less fluid and stiffer but obey to the same universal scaling law if excess area is taken correctly into account.

WHY IT MATTERS Mammalian cells are extremely soft and easily deformed. These properties are of utmost importance for many biological processes including cell migration, division, growth development, and carcinogenesis. Here, the rheological properties of a hidden, inaccessible cell surface—the basolateral membrane—are investigated with the help of an experimental trick. It was found that the basolateral membrane is substantially stiffer and less fluid than the apical membrane of epithelial cells. Thus, the polarity of the epithelial cells is also maintained at the mechanical level.

INTRODUCTION

Cellular polarity manifests itself at various levels such as organelle distribution, plasma membrane composition, and cytoskeletal architecture (1). Particularly, epithelial cells exhibit polarized formation of cell-cell junctions comprising adherens junctions and tight junctions separating the apical domain from the basolateral side (2,3). Many epithelial cells form microvilli at the apical domain filled with bundled actin filaments that increase the surface area substantially. On the basal side, stress fibers and focal adhesions emerge, responsible for attaching cells to the extracellular matrix. For confluent polar epithelial cells, our understanding of cell mechanics comes mainly from indentation experiments in which the apical side facing the culture medium has been studied (4–12), whereas very few studies have addressed the elastic properties of the basal side, let alone their dissipative properties (13–15). It is generally believed that the response of cells to deformation originates predominately from the cellular cortex consisting of a thin, contractile, and transiently cross-linked actin mesh connected to the plasma membrane (16–19). Prestress of the cortex is provided by motor proteins that, in conjunction with cross-linked actin, ensure resilience of the cell body on the one hand and fluidity of the cell to perform dynamic shape changes on the other hand (17–21). It was found that cells generally behave as a soft, glassy material giving rise to power law rheology with power law exponents between 0.2 and 0.4 because of the broad distribution of relaxation times (8,12,19,22–26). Many weak interactions are involved in the structure formation, which are independent of molecular details and make the

viscoelastic behavior appear unbound to a specific timescale.

Recently, we found that a linear viscoelastic continuum model of cortex based on power law rheology consistently explains the viscoelastic response of nonpolarized MDCK II cells, confluent cells, as well as apical cell membrane fragments over a wide time range (19,27). In particular, the defoliation of apical membranes by sandwich cleavage from living cells allowed to examine the impact of motor activity on fluidity (27). The method allows neglecting contributions from the cell interior, which include various filament types, organelles, and the densely packed cytoplasm that normally hinders the study of the cortex. Based on these experiments and data from of previous publications, I now revisited indentation-relaxation experiments of basolateral membranes from MDCK II cells grown on porous supports (5,13). I first present a comprehensive theoretical model based on free-energy minimization that describes the viscoelastic response of thin membranes to indentation with a conical indenter and in a second step compare the stiffness-fluidity relationship to that of living cells probed from the apical side.

I found that compared with the viscoelastic properties of confluent cells, isolated basal cortices are much stiffer and less fluid, but consistently follow the same universal scaling law when the excess area is properly accounted for.

MATERIALS AND METHODS

All experimental data were obtained from previous publications. Experimental force data from confluent MDCK II were taken from Pietuch et al. (5), whereas all data from basolateral membrane patches were published by Lorenz et al. (13) In these works, only the approach curves were evaluated using exclusively elastic tension models. Here, I included the available retraction curves in the comprehensive viscoelastic analysis. The following paragraphs repeat the key steps in obtaining these data.

Preparation of baslolateral membrane patches on porous substrates

Porous silicon substrates purchased from fluXXion B.V. were used as cell culture substrates. Pores possess a depth of 800 nm and display a diameter of 1.2 μm. The substrates were first coated with a thin adhesive layer of chromium (3 nm) followed by a gold coating of 60 nm, which has been proven to be an excellent surface for culturing MDCK II cells (28). Basolateral membrane fragments of MDCK II cells were obtained using a squirting-lysis protocol described previously (13,29). Confluent MDCK II cells were grown in minimal essential medium on porous substrates supplemented with 2 mM/L glutamine and 10% (v/v) fetal calf serum at $37°$ in an 95% air/5% CO_2 humidified incubator. Cells were subject to osmotic stress using hypotonic buffer. Shear stress by a buffer stream led to cleavage of the cells and also eventually to complete removal of the upper cell bodies.

Atomic force microscopy and indentation experiments

Atomic force microscopy (AFM) measurements were carried out with an MFP-3D microscope (Asylum Research, Santa Barbara, CA) at $20°C$ using MSCT cantilevers from Veeco with a nominal spring constant of 0.01 N/m. Ramp velocities were kept constant and set to 2 μm/s.

Theory

Here, I describe how force cycle experiments carried out with a conical indenter can be modeled with a minimum of essential assumptions to correctly access the viscoelastic properties of thin pore-spanning cortices. The viscoelastic parameters comprise a scaling factor (area compressibility modulus K_A^0), the prestress σ_0, and the fluidity β (power law exponent) of the membrane-cortex composite. The general geometry is schematically shown in Fig. 1 A. R denotes the radius of the pore and a is the contact radius of the membrane with the conical indenter.

Force response of viscoelastic cortices spanned over a pore

In contrast to our previous publication that facilitates the theoretical treatment by assuming that the AFM-indenter can be modeled by a cylindrical flat punch with a small radius of a few nanometers (27), I now consider a conical indenter and also abandoned the small gradient approximation, which is typically used to simplify the description of the force response (9,30−33). The following treatment is partly inspired by the work of Powers et al. (34) who dealt with the formation of tethers pulled from a planar membrane. The free energy of the membrane is given by (35,36)

$$\mathcal{E}_{el} = \int_S \left[\frac{\kappa}{2}(2H)^2 + \frac{\overline{\kappa}}{2}K + \sigma \right] dA, \tag{1}$$

where S is the surface of the membrane, H is its mean curvature $(2H = 1/R_1 + 1/R_2)$, and K is the Gaussian curvature $(K = (R_1R_2)^{-1})$. κ and $\overline{\kappa}$ are the splay and saddle splay moduli, respectively, i.e., essentially elastic constants. Although κ can easily be obtained experimentally and is always positive, $\overline{\kappa}$ is difficult to obtain. The Gaussian curvature is independent of how the surface is embedded in $\mathbb{R}^3$ and is an intrinsic property of the surface. According to the Gauss-Bonnet theorem, the integral of the Gaussian curvature over a surface depends only on its topology and boundary. This implies that for a closed surface the energy contribution of the Gaussian curvature during any deformation is constant unless the topology of the surface changes and can be ignored when determining the shape of the membrane. Because the membrane has edges, the Gaussian modulus affects the shape through the boundary conditions, which we will neglect for the sake of simplicity, i.e., we set $\overline{\kappa} = 0$ (34). σ denotes the surface tension, i.e., comprising mainly the free-energy contribution (per unit area) arising from adhesion of the cortex fragment to the pore rim, and in more general terms, it represents the chemical potential of the membrane reservoir. It can also be considered the Lagrangian multiplier to keep the area constant. The shape equation is obtained from standard variational calculus representing the balance of normal forces per unit area (37):

$$\Delta p - 2\sigma H + 2\kappa \left(\Delta H + 2H^3 - 2HK \right) = 0. \tag{2}$$

The pressure difference Δp enters as the Lagrange multiplier ensuring constant volume. For free-spanning membranes on pores
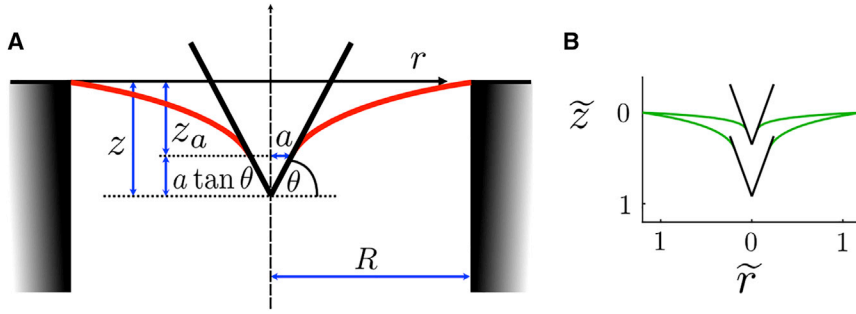
FIGURE 1 (*A*) Parametrization of the indentation experiment. The free membrane is in red color and the indenter in black. (*B*) General shape of the membrane (*green*) at two different indentation depths after minimizing the area.

open to both sides, we can discard this contribution for the free membrane as opposed to living cells. We assume that the energy contribution due to recruiting new surface area against the surface tension $\sigma \approx 10^{-3}$ N is substantially larger than the bending energy. Because κ is expected to be rather small, on the order of 10^{-19} J depending on the thickness d of the cortex ($\kappa \propto d^3$) and the lipid composition, we can assume that the dimensionless perturbation parameter $\varepsilon = \kappa/\sigma$ is indeed very small ($\approx 10^{-16}$ m^2). Thermal fluctuations are, therefore, negligible, and we can rewrite Eq. 2 (34):

$$2\varepsilon\left(\Delta H + 2H^3 - 2HK\right) - 2H = 0. \tag{3}$$

Assuming that $\varepsilon = 0$, we obtain $H = 0$, the minimal surface equation, which provides essentially the shape of a catenoid because this is the only nonplanar minimal surface with zero mean curvature. It is, however, immediately clear that this simplified differential equation is not entirely compatible with the boundary condition, because ε is multiplied with the highest derivative of H (34). Precisely, an external force is balanced by curvature in which the indenter meets the membrane $r = a$ implying that $H \neq 0$. In contrast, the boundary condition $\sigma H = 0$ at $r = R$, the pore rim, is compatible with the differential equation as the pore rim acts as a hinge. Employing the concept of perturbation theory, we therefore need to consider a boundary layer at the contact line with the indenter rendering outer ($r > \delta$) and inner ($r < \delta$) solutions incompatible. The outer solution of the free membrane is a catenoid held between two circular boundaries, one being the pore with a large radius R and the smaller one defined by the contact with the conical indenter at $r = a$. The thickness of the boundary layer $\delta = \sqrt{\kappa/\sigma}$ can be inferred from equating $\varepsilon\Delta H$ with H and represents a characteristic length scale. On scales larger than δ, tension dominates, whereas on smaller length scales, bending is the most important energy contribution. In our case, δ is on the order of 10 nm; therefore, it is considered small compared with size of the free membrane. In the following paragraphs, we will only consider the dominant outer solution because the characteristic length scale is governed by the surface tension due to the thin membrane patches and the large adhesion forces.

The problem of finding the shape $r(z)$ of the membrane during indentation therefore reduces to the problem of finding its minimal free surface (34,38). We first consider the elementary case of two rings of equal size separating the membrane by $2L$ to form a shape with zero mean curvature. The area element $dA = 2\pi r ds$ generates the surface through the integral equation:

$$A = \int 2\pi r \, ds = 2\pi \int_{-L}^{+L} r\sqrt{1 + r'^2}\,dz, \tag{4}$$

with $r' = dr/dz$. Using standard techniques of variational calculus, we arrive at the following equation (38):

$$r r'' = 1 + r'^2. \tag{5}$$

The differential equation can be integrated in two consecutive steps (38). Using $(1 + r'^2)' = 2r'r''$, we obtain the following equation:

$$r = r_N \sqrt{1 + r'^2}, \tag{6}$$

with r_N being a constant. Second, we employ the identity, which is conveyed by the following equation:

$$r = r_N \cosh\left(\frac{z - C}{r_N}\right), \tag{7}$$

with the integration constant C being 0 for two equally sized rings (38). Because we have one radius given by the pore rim R and the other one by the contact radius a we need to infer C from this boundary condition. r_N is identified as the minimal radius of the catenoid, its so-called neck radius. C can be obtained from $r = R$ of the upper rim,

$$C = \pm r_N \cosh^{-1}(R / r_N), \tag{8}$$

leading to the following equation:

$$r(z) = r_N \cosh\left(\frac{z}{r_N}\right) \mp \sqrt{1 - r_N^2}\sinh\left(\frac{z}{r_N}\right). \tag{9}$$

The upper sign corresponds to catenaries with a minimal neck radius at a positive value of z ($C > 0$), the indentation depth. Conversely, for $z(r)$, the shape equation of the free membrane, we can write the following:

$$z(r) = r_N \cosh^{-1}\left(\frac{r}{r_N}\right) + r_N \cosh^{-1}\left(\frac{R}{r_N}\right), \tag{10}$$

or in nondimensional form ($\tilde{z} = z/R$, $\tilde{r}_N = r_N/R$, $\tilde{r} = r/R$),

$$\tilde{z}(\tilde{r}) = \tilde{r}_N \cosh^{-1}\left(\frac{\tilde{r}}{\tilde{r}_N}\right) + \tilde{r}_N \cosh^{-1}\left(\frac{1}{\tilde{r}_N}\right). \tag{11}$$

A simple relation holds between r_N, the minimal radius, and the force f:

$$f = -\frac{\partial E}{\partial z} = -\frac{\partial \left(2\pi\sigma \int_0^{z_a} r\sqrt{1+r'^2}\,dz\right)}{\partial z} = -\frac{2\pi\sigma r}{\sqrt{1+r'^2}},$$ (12)

with z_a the indentation depth at $r = a$. At the neck of the catenoid $r = r_N$, we have $r' = 0$ and therefore $r_N = f/(2\pi\sigma)$. Because at $r(z_a) = a$ with $a > r_N$, we can write the following:

$$z_a = r_N \ln\left(\frac{a \pm \sqrt{a^2 - r_N^2}}{1 - \sqrt{1 - r_N^2}}\right).$$ (13)

Equation 13 is responsible for two branches, forming a closed curve in the $f - z_a$ plane for $a < R$ (34). In principle, a critical (maximal) separation z_a exists in which no solution is found, i.e., the catenoid becomes unstable and breaks. If the contact radius a is fixed and the indentation depth below the maximum (before instability) two catenoidal equilibrium solutions exist (see Eq. 13). We only have to consider the branch (minus sign in Eq. 13) with a larger $\tilde{r}_N$-value that has less area. The other branch is not found for real minimal surfaces. Therefore, we proceed with the minus sign in Eq. 13. The existence of an elastic boundary layer allows the limit of a point force, i.e., $a \to 0$, which is in contrast to pure soap films. In practice, however, point forces do not play a role because conventional AFM tips display curvature radii of ~20 nm. Now, we only have to determine the contact radius a from the continuity condition, where the slope is identical for indenter and freestanding membrane. For a conical indenter we find the following:

$$\left.\frac{dz(r)}{dr}\right|_{r=a} = \frac{1}{\sqrt{\left(\frac{a}{r_N}\right)^2 - 1}} = -\tan\theta,$$ (14)

with $\pi/2 - \theta$ being the half-opening angle of the cone, giving

$$a = \sqrt{\left(\frac{r_N}{-\tan\theta}\right)^2 + r_N^2},$$ (15)

and the indentation depth at the tip of the indenter is $z(r=0) = z_a + a\tan(\theta)$. Note that $a > r_N$ as r_N is the smallest possible radius of a catenoid. The tension of the membrane is not necessarily a constant but depends on the area dilatation, which inevitably occurs upon indentation:

$$\sigma = \sigma_0 + K_A\alpha,$$ (16)

with σ_0 the initial prestress and K_A the area compressibility modulus. $\alpha = \frac{A - A_0}{A_0}$ denotes the relative area dilatation with A the actual area and A_0 the area before indentation, i.e., $A_0 = \pi R^2$. The actual area of the free membrane forming the catenoid is

$$A_{cat} = \frac{\pi r_N^2}{2}(\sinh(2z_a / r_N) + 2C - \sinh(2C) + 2z_a / r_N),$$ (17)

with $C = -\cosh^{-1}(R / r_N)$. Additionally, we need to consider coating of the cone up to $r = a$, leading to $A_{cone} = \pi a^2/\cos(\theta)$, and therefore,

the overall area of the membrane is $A = A_{cone} + A_{cat}$. If excess membrane area A_{ex} is recruited from the pore rim, we refer to an apparent compressibility module $K_A \frac{A_0}{A_0 + A_{ex}}$ (vide infra).

As shown previously, viscoelasticity enters through the time dependency of the area compressibility modulus $K_A = K_A^0\left(\frac{t}{t_0}\right)^{-\beta}$ with $0 \le \beta \le 1$ and $t_0 = 1s$ (set arbitrarily) (19). The power law indicates that relaxation is not tied to an internal timescale (22). Consequently, the elastic-viscoelastic-correspondence principle leads to the following expression for the overall tension:

$$\sigma(t) = \sigma_0 + \int_0^t K_A^0\left(\frac{t-\tau}{t_0}\right)^{-\beta}\frac{\partial\alpha(\tau)}{\partial\tau}\,d\tau.$$ (18)

Because viscoelasticity of the membrane-cortex composite impacts only the in-plane area compressibility modulus, we can safely assume that the contour during indentation is identical to the contour for the elastic case. In nondimensional form ($\tilde{a} = a/R$) the indentation depth at $r = 0$ is

$$\tilde{z} = \tilde{r}_N\ln\left(\frac{\tilde{a} - \sqrt{\tilde{a}^2 - \tilde{r}_N^2}}{1 - \sqrt{1 - \tilde{r}_N^2}}\right) + \tilde{a}\tan(\theta),$$ (19)

which tells us that for a given indenter geometry, i.e., θ-value, the shape of the membrane and its scaled force response is uniquely defined by the distance between the two rings (In the limit of small forces Eq. 19 reduces to $\tilde{z} = \tilde{r}_N\ln\tilde{a}^{-1} + \tilde{a}\tan(\theta)$, identical to the small gradient solution $\sigma\nabla^2 u = q(r)$ with $q(r)$ the transverse load on the membrane being zero for $a < r < R$ and $f/\pi a^2$ at $r = a$.[9] At large forces the deviations are substantial, leading to an overestimation of force response by the membrane for the small gradient approximation.). The same is naturally true for the surface integral. This allows us to numerically compute $\tilde{z}(\tilde{r}_N)$ as well as $\alpha(\tilde{r}_N)$ for each value of θ once and for all and fit the two curves with two polynomials, $\tilde{g}(\tilde{z}, \Theta) = \sum_n c_n\tilde{z}^n$ and $\alpha(\tilde{z}, \Theta) = \sum_n d_n\tilde{z}^n$, respectively. This permits us to obtain an analytical solution of the corresponding elastic-viscoelastic problem for indentation (approach),

$$f_{app} = 2\pi\tilde{g}(\tilde{z}, \Theta)R\left(\sigma_0 + \int_0^t K_A(t-\tau)\frac{\partial\alpha(\tau)}{\partial\tau}\,d\tau\right),$$ (20)

and relaxation (retraction) starting at $t = t_m$,

$$f_{ret} = 2\pi\tilde{g}(\tilde{z}, \Theta)R\left(\sigma_0 + \int_0^{t_m} K_A(t-\tau)\frac{\partial\alpha(\tau)}{\partial\tau}\,d\tau\right)$$ (21)

respectively. Here, I assumed that in-plane stretching of the membrane/cortex is time-dependent $\alpha(\tilde{z}(t))$ as we apply a linear ramp $\tilde{z}(t) = \tilde{v}_0 t$ at the approach and $\tilde{z}(t) = \tilde{v}_0(2t_m - t)$ upon retraction, respectively ($\tilde{v}_0 = v_0/R$). Hereditary integrals using a polynomial to the order n for $\alpha(t)$ are readily solved:

$$f_{app} = 2\pi\tilde{g}(\tilde{z}, \Theta)R\left(\sigma_0 + K_A^0\sum_n d_n\frac{t^{-\beta}n(\tilde{v}_0 t)^n\Gamma(1-\beta)\Gamma(n)}{\Gamma(1-\beta+n)}\right),$$ (22)

and

$$f_{\text{ret}} = 2\pi\tilde{g}(\tilde{z},\Theta)R\left(\sigma_0 + K_A^0\sum_n d_n\left[t^{-\beta}(t_m\tilde{v}_0)^n{}_2F_1\left(\beta,n;n+1;\frac{t_m}{t}\right) + \frac{(-1)^\beta\Gamma(\beta+1)\Gamma(n)\left(\frac{1}{2t_m-t}\right)^{-\beta}(-\tilde{v}_0(t-2t_m))^n}{\Gamma(\beta+n+1)}\right.\right.$$

$$\left.\left.-\frac{(t-t_m)^\beta\left(\frac{t-t_m}{t-2t_m}\right)^{-\beta}(t_m\tilde{v}_0)^n{}_2F_1\left(-\beta,n;n+1;-\frac{t_m}{t-2t_m}\right)}{n}\right]\right) \tag{23}$$

with the Gamma function $\Gamma(n) = \int_0^\infty x^{n-1}e^{-x}dx$, and the ordinary hypergeometric function ${}_2F_1(a,b;c;z)$. Usually, polynomials to the order of $n = 4$ are sufficient to describe the functions $\tilde{g}(\tilde{z},\Theta)$ and $\alpha(\tilde{z},\Theta)$ with good accuracy. Experimental force time curves were subject to fitting a piece-wise function $f(t \leq t_m) = f_{\text{app}}(t)$ and $f(t > t_m) = f_{\text{ret}}(t)$.

Force response of living cells

We use the model of Hubrich et al. to fit the data (27). In brief, confluent cells are considered to be capped cylinders with contact angles around $\phi_0 = 35°$ before deformation (5). Generally, we treat the cell as a liquid-filled object surrounded by an isotropic viscoelastic shell deformed at constant volume. The force f acting on the apex of the cell is shown below (27):

$$f = 2\pi\left(R_1^2\left(\frac{R_1\sin(\phi) + a\sin(\Theta)}{R_1^2 - a^2}\right) - R_1\sin\phi\right)\sigma(t), \tag{24}$$

or in nondimensional form ($\tilde{f} = f/(2\pi R_1\sigma(t))$, $\tilde{a} = a/R_1$, $\tilde{z} = z/R_1$),

$$\tilde{f} = \frac{\sin(\phi) + \tilde{a}\sin(\Theta)}{1 - \tilde{a}^2} - \sin\phi = \tilde{g}(\Theta,\phi,z), \tag{25}$$

with R_1 as the radius at the base of the spherical cap and ϕ as the contact angle in response to deformation (5). For a given set of angles ϕ and Θ, the generic shape function $\tilde{g}(\Theta,\phi,z)$ is computed numerically and the outcome fitted by a polynomial $\tilde{g}(\Theta,\phi_0,z) = \sum_n c_n\tilde{z}^n$ to obtain the coefficients c_n. Computation of area change has been outlined before and the outcome approximated with a polynomial as described above $\tilde{\alpha}(\Theta,\phi_0,z) = \sum_n d_n\tilde{z}^n$ to determine d_n, respectively (5,27).

Viscoelasticity of the shell enters through Eq. 18, replacing $\sigma(t)$ as before. What follows is numerical solution of a set of nonlinear equations for the shape of the deformed cell to fulfill force balances and the constant volume boundary condition (27). For a given indenter geometry and contact angle ϕ_0, this has to be solved only once and scaling is accomplished by multiplication with R_1.

RESULTS AND DISCUSSION

Previously, we investigated the topography and elastic properties of basolateral membranes derived from confluent MDCK II cells grown on porous substrates (13). Defoliation was accomplished according to the squirting lysis protocol, in which the confluent MDCK II cells were first subject to osmotic swelling with addition of hypotonic buffer (Fig. 2 A) (13,29). Subsequently, the cells were ruptured by applying a gentle buffer stream from a syringe directed to the cell monolayer at an angle of 45°. After removal of cell debris, pore-spanning basolateral membranes were obtained as shown in Fig. 2, C and D. After imaging, force cycle curves were collected from the center of the pore. The exact positioning of the AFM tip over the center of the pore was accomplished by first mapping the area of interest and then addressing the pore center from the obtained coordinates. In particular, inaccurate positioning leads to response functions that appear to correspond to stiffer sheets. A force-volume protocol (39) was also frequently used, and the force curves were selected accordingly. The indentation curves obtained from the pore's center were previously described using an asymptotic linear relationship between force and indentation depth essentially capturing only the prestress of the cortex (13).

I now reevaluated this data, including the retraction curves that were not considered in the previous publication, by applying the viscoelastic model described above. Both indentation and relaxation were fitted, with Eqs. 22 and 23 as a piece-wise function providing access to three relevant mechanical parameters, the prestress σ_0, the scaling factor (apparent area compressibility modulus) K_A^0 and the fluidity or power law exponent β, the latter two, as we shall see, being not independent (Fig. 2 D). It is important to notice that for pore-spanning membranes and cortices, the prestress σ_0 corresponds mainly to the differential adhesion free energy between the pore rims G_{pr} and the free-standing part G_p:

$$\sigma_0 = \frac{G_{\text{pr}} - G_p}{\pi R^2}. \tag{26}$$

The area compressibility modulus is the response function of the linear-elastic resistance of the
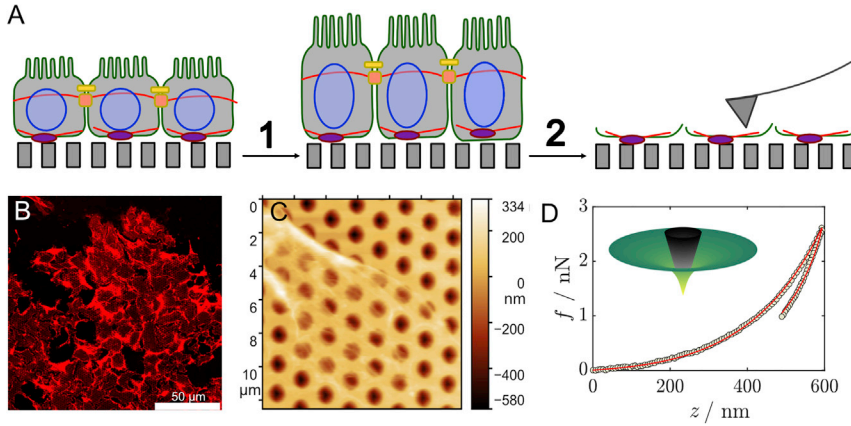
FIGURE 2 (*A*) Preparation of basolateral membrane sheets on porous supports (13). MDCK II cells are first grown to confluence on a porous support with pores of 1.2 μm in diameter. After exposing the cells to hypotonic solution (1), the swelling makes them susceptible for shear stress (2) applied by a buffer stream. The isolated membranes were subject to indentation experiments using a conventional AFM instrument. (*B*) Fluorescence micrograph showing the results of the squirting-lysis protocol (TRITC: phalloidin-stained actin filaments). (*C*) AFM image showing actin stress fibers. (*D*) Typical force cycle curve (*circles*) subject to fitting of equations (22, 23) (*red line*). Fitting range was limited to avoid interference from adhesion events. The inset shows the shape of the membrane at largest indentation depth.

cortex/membrane assembly against in-plane area dilatation. Depending on the boundary conditions, area dilatation occurs inevitably during deformation as required for deviation from a minimal surface. Although cells maintain a constant volume during deformation, the basal membrane sheets are physically and chemically attached to the pore rims: the strength of attachment given by Eq. 26 (9,19,28). The measured area compressibility modulus of the basolateral membrane sheets contains contributions from the rather inextensible membrane and the actin mesh. Albeit the outstretched plasma membrane is almost inextensible exhibiting considerably large K_A-values of 0.1−0.5 N/m depending on the lipid composition (40), excess membrane area A_{ex} can be recruited from wrinkles, ruffles, folds, and, eventually, the entire footprint of the cell during indentation. This excess area diminishes the measured area compressibility by a factor of $A_0/(A_0 + A_{ex})$. Consequently, experiments with neat lipid bilayers neither display a measurable area compressibility modulus nor a noticeable hysteresis during relaxation because the excess area recruited from adjacent surface is often extremely large and friction between the pore rim and the bilayer small (33). The second contribution to K_A comes from the underlying actin cortex, which points toward the indenter in this case. Notably, recruitment of excess area from the adjacent surface is also possible in this case, giving also rise to apparent values (vide infra), which are much smaller than those obtained by assuming only the area of a single pore. As pointed out previously, knowledge of cortex thickness and mesh size allows to roughly estimate the elastic modulus of a cross-linked actin network (19,41):

$$K_A \approx \frac{3k_B T l_p^2}{\zeta^2} \frac{d}{l_c^3}, \quad (27)$$

with the distance between cross-links $l_c \approx \zeta^{4/5} l_p^{1/5}$ and the persistence length l_p (41). Assuming reasonable values for the mesh size of $\zeta = 100$ nm, a cortex thickness *d* of 150 nm and a persistence length of 17 m (42) we obtain K_A-values of ~2.5 mN/m. Taken together, we expect rather small values for the area compressibility due to the presence of excess area. Notably, in the previous publication we removed filamentous actin partly resulting in a substantial softening of the membrane patch confirming the importance of the cortex for the elastic response (13).

The power law exponent β represents the flow behavior of the cortex. If β is close to 0, the cortex behaves as an elastic solid, whereas a β-value of 1 corresponds to a Newtonian liquid. Generally, intermediate β-values are found for living cells. It could be shown that β is not independent of the corresponding elastic modulus or scaling factor in the case of power law rheology, which in our case is the apparent area compressibility modulus K_A^0, but decreases according to $\beta \propto -\log K_A^0$ (vide infra) (19).

Fig. 2 *D* shows a typical force cycle curve consisting of an approach curve generated by a linear ramp and a subsequent relaxation also following a linear ramp (identical approach and retraction velocity) obtained by probing a basolateral membrane patch. The patch covering the pore was indented as precisely as possible in the center fulfilling the axial symmetry conditions of the theory. Because of the potential for adhesion events to affect the retraction curve, only a portion of the retraction curve (approximately one-third) was considered for fitting.

Fig. 3 shows the results of fitting Eqs. 22, 23 to many experimental force curves obtained from basolateral membrane patches of adherent MDCK II cells. Generally, three parameters are obtained from the entire force cycle, the scaling factor K_A^0, the prestress σ_0 and the fluidity (power law exponent) β. The mean
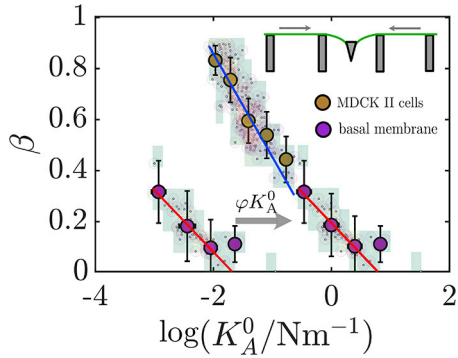
FIGURE 3   Fluidity β as a function of area compressibility K_A^0 for basolateral membrane sheets (*purple*) and living cells probe from the apical side (*brown*). The data for living cells were obtained from reevaluating experiments by Pietuch et al. (5) using the model of Hubrich et al. (27) The arrow illustrates what happens to the data if K_A^0 is rescaled by the average area of a membrane footprint, the flow illustrated by the inset in the top right corner.

prestress $\overline{\sigma}_0$ was found to be around 1.6 ± 1 mN/m, which I largely attribute to differential adhesion at the pore rim and stress exerted by actin bundles. The large variance is due to substantial pore to pore variation supporting the theory of differential adhesion that can locally be quite different, for instance in the vicinity of focal contacts. The mean fluidity was considerably lower ($\beta \approx 0.2$) than reported for confluent living cells evaluated with the Evans model ($\beta \approx 0.6$) (19,27). This is attributed mainly to the missing sliding action of myosin motors compared with living cells, where motor proteins maintain fluidity of the cortex. It is also conceivable that the basolateral cortex is potentially stiffer than the apical side, but a previous study has shown that membrane extracts actually have lower fluidity (27). An increase of prestress due to the presence of pore rims (Eq. 26) compared with the cortex stress of living cells can easily generate a substantial decrease of fluidity (19,23,43).

Most importantly, however, a linear decrease of β with the scaling factor $\log K_A^0$ was found as reported from the rheology of living cells and apical membrane fragments (22,23,27). Because β and K_A^0 depend on each other in this way, it implies automatically that stiffer cortices are also less fluid and vice versa. This universal law has first been discovered by Fabry et al. using ferrimagnetic beads adhering to the actin cytoskeleton and actuated by an external magnetic field (22). A weak power law was observed for G' being larger than G'' below 300 Hz. The spectra were described by a structural damping model that produced parameters falling onto such a master curve. This essentially suggested that the constitutive elastic and frictional properties are controlled by a single parameter, for instance, β, over a wide frequency range (22). Thus, in principle, the cells can respond to external

cues by modulating solely β as the primary control parameter. However, if the data are extrapolated to a fully elastic material ($\beta = 0$, intersection with the x axis) the basolateral membranes exhibit a very low stiffness compared with living cells (Fig. 3) (27). This needs further exegesis. If one takes into account that the excess area might be as large as the patch itself including hidden reservoirs $A_{ex} \approx 329 \pm 49$ μm (44) because upon indentation the cortex can follow the indenter into the pore, the corrected (see *arrow* in Fig. 3) correlation (φK_A^0 with $\varphi = \frac{A_0 + A_{ex}}{A_0}$) continues the scaling found for living cells probed at the apical side (Fig. 3). Therefore, the master curve still holds and considering only one parameter, the fluidity β, is sufficient. The lack of functional motor proteins could be responsible for the flatter slope found for the basolateral membrane patches compared with that of living cells. This was shown recently for apical cell membrane fragment after addition of exogenous ATP to revive some of the remaining myosin motors significantly increasing fluidity of the cortex (27). Close to $\beta \approx 0$, the elastic limit, other contributions such as friction between the membrane and the pore rim might become visible: an explanation of why energy losses occur even with very high stiffness. A direct comparison between cortex fragments derived either from the basolateral or the apical side shows that polarity has only a small impact on viscoelasticity. Hubrich et al. (27) found that apical membrane fragments also exhibit low fluidity in the range of 0.2 similar to what was found here, whereas living cells display substantially higher fluidity presumably due to motor activity as mentioned above. Along the same lines, Kim et al. found only small differences in elasticity of PaTu8988S and PaTu8988T probed either from the basal or apical side, respectively (15).

Notably, the presence of pores during cell culture renders MDCK generally softer than cultured on continuous stiff surfaces such as culture dishes or silica. This was recently shown in a systematic fashion using different pore sizes (45). The area compressibility modulus might be reduced by a factor of 2−3 comparing cells cultured on flat substrates with those grown on porous surfaces with a pore diameter of 5 μm (45).

In conclusion, for the first time, to my knowledge, it was possible to obtain the viscoelastic properties of basolateral membranes in the absence of other cellular ingredients by site-specific indentation-relaxation experiments of planar membrane patches on porous substrates. The theoretical model to describe the force cycles correctly describes the shape of the free membrane/cortex in terms of a minimal surface and permits to easily modify the constitutive equations to capture dissipative processes in thin films employing the

viscoelastic-elastic correspondence principle (8). It could be shown that the universal scaling law between stiffness of cells and their fluidity is largely preserved, implying that cell cortices cannot change their elastic and dissipative properties independently (19,22,23). A decrease of stiffness is always accompanied by an increase in fluidity. We found that regulation of mechanical properties can also be accomplished via storage of excess area to soften the apparent moduli over orders of magnitude. The cortex fragments are stiffer, and less fluid compared with living cells that can be partly attributed to arrested myosin motors but could also be a consequence of polarity and therefore larger prestress exerted by stress fibers at the basal side. Although for unstressed actin networks, a power law exponent of 0.5 is expected, I found substantially lower values of only 0.2 (46). I attribute this partly to higher prestress and missing motor activity that decreases the noise level necessary to drive the cytoskeleton into a disordered state that eventually enables the cells to perform tasks like spreading, migration, and division.

Polarity of epithelial cells is very pronounced on many levels, and cortical viscoelasticity seems to be no exception. However, more experiments involving fully active cortices with myosin motors are needed to obtain a more comprehensive picture of viscoelasticity in the context of cell polarity.

ACKNOWLEDGMENTS

DECLARATION OF INTERESTS

The author declares no competing interests.

REFERENCES

1. Rodriguez-Boulan, E., and I. G. Macara. 2014. Organization and execution of the epithelial polarity programme. *Nat. Rev. Mol. Cell Biol.* 15:225–242.

2. Niessen, C. M., D. Leckband, and A. S. Yap. 2011. Tissue organization by cadherin adhesion molecules: dynamic molecular and cellular mechanisms of morphogenetic regulation. *Physiol. Rev.* 91:691–731.

3. Shin, K., V. C. Fogg, and B. Margolis. 2006. Tight junctions and cell polarity. *Annu. Rev. Cell Dev. Biol.* 22:207–235.

4. Sen, S., S. Subramanian, and D. E. Discher. 2005. Indentation and adhesive probing of a cell membrane with AFM: theoretical model and experiments. *Biophys. J.* 89:3203–3213.

5. Pietuch, A., B. R. Brückner, …, A. Janshoff. 2013. Elastic properties of cells in the context of confluent cell monolayers: impact of tension and surface area regulation. *Soft Matter.* 9:11490.

6. Rother, J., H. Nöding, …, A. Janshoff. 2014. Atomic force microscopy-based microrheology reveals significant differences in the viscoelastic response between malign and benign cell lines. *Open Biol.* 4:140046.

7. Cartagena-Rivera, A. X., J. S. Logue, …, R. S. Chadwick. 2016. Actomyosin Cortical Mechanical Properties in Nonadherent Cells Determined by Atomic Force Microscopy. *Biophys. J.* 110:2528–2539.

8. Brückner, B. R., H. Nöding, and A. Janshoff. 2017. Viscoelastic Properties of Confluent MDCK II Cells Obtained from Force Cycle Experiments. *Biophys. J.* 112:724–735.

9. Nehls, S., and A. Janshoff. 2017. Elastic Properties of Pore-Spanning Apical Cell Membranes Derived from MDCK II Cells. *Biophys. J.* 113:1822–1830.

10. Krieg, M., G. Fläschner, …, D. J. Müller. 2018. Atomic force microscopy-based mechanobiology. *Nat. Rev. Phys.* 1:41–57.

11. Garcia, P. D., and R. Garcia. 2018. Determination of the viscoelastic properties of a single cell cultured on a rigid support by force microscopy. *Nanoscale.* 10:19799–19809.

12. Garcia, P. D., C. R. Guerrero, and R. Garcia. 2020. Nanorheology of living cells measured by AFM-based force-distance curves. *Nanoscale.* 12:9133–9143.

13. Lorenz, B., I. Mey, …, A. Janshoff. 2009. Elasticity mapping of pore-suspending native cell membranes. *Small.* 5:832–838.

14. Gudzenko, T., and C. M. Franz. 2013. Inverting adherent cells for visualizing ECM interactions at the basal cell side. *Ultramicroscopy.* 128:1–9.

15. Kim, J. H., K. Riehemann, and H. Fuchs. 2018. Force Spectroscopy on a Cell Drum: AFM Measurements on the Basolateral Side of Cells via Inverted Cell Cultures. *ACS Appl. Mater. Interfaces.* 10:12485–12490.

16. Fischer-Friedrich, E., Y. Toyoda, …, F. Jülicher. 2016. Rheology of the Active Cell Cortex in Mitosis. *Biophys. J.* 111:589–600.

17. Chugh, P., A. G. Clark, …, E. K. Paluch. 2017. Actin cortex architecture regulates cell surface tension. *Nat. Cell Biol.* 19:689–697.

18. Chugh, P., and E. K. Paluch. 2018. The actin cortex at a glance. *J. Cell Sci.* 131:jcs186254.

19. Cordes, A., H. Witt, …, A. Janshoff. 2020. Prestress and Area Compressibility of Actin Cortices Determine the Viscoelastic Response of Living Cells. *Phys. Rev. Lett.* 125:068101.

20. Salbreux, G., G. Charras, and E. Paluch. 2012. Actin cortex mechanics and cellular morphogenesis. *Trends Cell Biol.* 22:536–545.

21. Fritzsche, M., C. Erlenkämper, …, K. Kruse. 2016. Actin kinetics shapes cortical network structure and mechanics. *Sci. Adv.* 2:e1501337.

22. Fabry, B., G. N. Maksym, …, J. J. Fredberg. 2001. Scaling the microrheology of living cells. *Phys. Rev. Lett.* 87:148102.

23. Kollmannsberger, P., and B. Fabry. 2011. Linear and Nonlinear Rheology of Living Cells. *Annu. Rev. Mater. Res.* 41:75–97.

24. Kollmannsberger, P., C. T. Mierke, and B. Fabry. 2011. Nonlinear viscoelasticity of adherent cells is controlled by cytoskeletal tension. *Soft Matter.* 7:3127–3132.

25. Zhou, E. H., F. D. Martinez, and J. J. Fredberg. 2013. Cell rheology: mush rather than machine. *Nat. Mater.* 12:184–185.

26. Sollich, P., F. Lequeux, …, M. E. Cates. 1997. Rheology of Soft Glassy Materials. *Phys. Rev. Lett.* 78:2020–2023.

27. Hubrich, H., I. P. Mey, …, A. Janshoff. 2020. Viscoelasticity of Native and Artificial Actin Cortices Assessed by Nanoindentation Experiments. *Nano Lett.* 20:6329–6335.

28. Rouven Brückner, B., A. Pietuch, …, A. Janshoff. 2015. Ezrin is a Major Regulator of Membrane Tension in Epithelial Cells. *Sci. Rep.* 5:14700.

29. Ziegler, U., A. Vinckier, …, P. Groscurth. 1998. Preparation of basal cell membranes for scanning probe microscopy. *FEBS Lett.* 436:179–184.

30. Norouzi, D., M. M. Müller, and M. Deserno. 2006. How to determine local elastic properties of lipid bilayer membranes from atomic-force-microscope measurements: a theoretical analysis. *Phys. Rev. E Stat. Nonlin. Soft Matter Phys.* 74:061914.

31. Steltenkamp, S., M. M. Müller, …, A. Janshoff. 2006. Mechanical properties of pore-spanning lipid bilayers probed by atomic force microscopy. *Biophys. J.* 91:217–226.

32. Mey, I., M. Stephan, …, A. Janshoff. 2009. Local membrane mechanics of pore-spanning bilayers. *J. Am. Chem. Soc.* 131:7031–7039.

33. Mey, I., C. Steinem, and A. Janshoff. 2012. Biomimetic functionalization of porous substrates: towards model systems for cellular membranes. *J. Mater. Chem.* 22:19348.

34. Powers, T. R., G. Huber, and R. E. Goldstein. 2002. Fluid-membrane tethers: minimal surfaces and elastic boundary layers. *Phys. Rev. E Stat. Nonlin. Soft Matter Phys.* 65:041901.

35. Canham, P. B. 1970. The minimum energy of bending as a possible explanation of the biconcave shape of the human red blood cell. *J. Theor. Biol.* 26:61–81.

36. Helfrich, W. 1973. Elastic properties of lipid bilayers: theory and possible experiments. *Z. Naturforsch. C.* 28:693–703.

37. Zhong-can, O.-Y., and W. Helfrich. 1989. Bending energy of vesicle membranes: General expressions for the first, second, and third variation of the shape energy and applications to spheres and cylinders. *Phys. Rev. A Gen. Phys.* 39:5280–5288.

38. Cassel, K. W. 2013. Variational Methods with Applications in Science and Engineering. Cambridge University Press.

39. Kocun, M., T. D. Lazzara, …, A. Janshoff. 2011. Preparation of solvent-free, pore-spanning lipid bilayers: modeling the low tension of plasma membranes. *Langmuir.* 27:7672–7680.

40. Daily, B., E. L. Elson, and G. I. Zahalak. 1984. Cell poking. Determination of the elastic area compressibility modulus of the erythrocyte membrane. *Biophys. J.* 45:671–682.

41. Gardel, M. L., J. H. Shin, …, D. A. Weitz. 2004. Elastic behavior of cross-linked and bundled actin networks. *Science.* 304:1301–1305.

42. Ott, A., M. Magnasco, …, A. Libchaber. 1993. Measurement of the persistence length of polymerized actin using fluorescence microscopy. *Phys. Rev. E Stat. Phys. Plasmas Fluids Relat. Interdiscip. Topics.* 48:R1642–R1645.

43. Mulla, Y., F. C. MacKintosh, and G. H. Koenderink. 2019. Origin of Slow Stress Relaxation in the Cytoskeleton. *Phys. Rev. Lett.* 122:218102.

44. Butor, C., and J. Davoust. 1992. Apical to basolateral surface area ratio and polarity of MDCK cells grown on different supports. *Exp. Cell Res.* 203:115–127.

45. Rother, J., M. Büchsenschütz-Göbeler, …, A. Janshoff. 2015. Cytoskeleton remodelling of confluent epithelial cells cultured on porous substrates. *J. R. Soc. Interface.* 12:20141057.

46. Broedersz, C. P., M. Depken, …, F. C. MacKintosh. 2010. Cross-link-governed dynamics of biopolymer networks. *Phys. Rev. Lett.* 105:238101.